공학석사 학위논문

A new Mg-ion intercalation host of $LiNi_{0.5}Co_{0.2}Mn_{0.3}O_2$ as cathode materials for rechargeable Mg batteries

마그네슘이차전지용 마그네슘 이온 삽입이 가능한

새로운 구조의 $LiNi_{0.5}Co_{0.2}Mn_{0.3}O_2$ 양극 소재 연구

2016 년 8 월

서울대학교 대학원

재료공학부

조 용 범

A new Mg-ion intercalation host of $LiNi_{0.5}Co_{0.2}Mn_{0.3}O_2$ as cathode materials for rechargeable Mg batteries

마그네슘이차전지용 마그네슘 이온 삽입이 가능한

새로운 구조의 $LiNi_{0.5}Co_{0.2}Mn_{0.3}O_2$ 양극 소재 연구

지도 교수 강 기 석

이 논문을 공학석사 학위논문으로 제출함

2016 년 6월

서울대학교 대학원

재료공학부

조 용 범

조 용 범의 석사 학위논문을 인준함

2016 년 06 월

위 원 장 박 병 우 (인)

부위원장 강 기 석 (인)

위 원 남 기 태 (인)

Abstract

A new Mg-ion intercalation host of $LiNi_{0.5}Co_{0.2}Mn_{0.3}O_2$ as cathode materials for rechargeable Mg batteries

Cho, Yongbeom
Department of Material Science and Engineering
College of Engineering
The Graduate School
Seoul National University

Mg rechargeable battery is one of the most promising next-generation batteries on the merits of its high theoretical capacity, low cost and safety. However, searching new cathode materials with high energy density has been a great challenge so far due to the sluggish diffusion kinetics of divalent Mg^{2+} ions in the crystal structure of electrode materials. In this study, we utilize $LiNi_{0.5}Co_{0.2}Mn_{0.3}O_2$ (NCM523), which is widely used electrode material for Li-ion batteries (LIBs), as a cathode material for Mg rechargeable battery. We first discover that NCM523 can be a Mg intercalation host with high energy density along with the water-induced phase transformation from O3 to P3

layered structure. The water-intercalated P3 phase delivers the highest $Ni^{2+}/Ni^{3+}/Ni^{4+}$ redox potential of 3.1 V *vs.* Mg/Mg^{2+} yet reported for Mg cathode materials, with high energy density of 589 Wh kg^{-1}. This unusual behavior in NCM layered oxide, proposed in this work, provides an insight into designing promising cathode materials for Mg rechargeable battery.

Keywords: Mg rechargeable batteries; layered oxide; P3 phase; water; magnesiation
Student Number: 2014-21441

Contents

Abstract ……..…….. i

Contents ……..……...iii

List of Tables ……..…….. v

List of Figures ……vi

Chapter 1 Introduction ……..…1

1.1 Motivation and outline ……..…1

Chapter 2 Reaserch backgrounds …… 4

2.1. Introduction to Mg rechargeable batteries ……4

2.2. Layered oxide ……..…… 5

Chapter 3 Experimental……8

3.1. Characterization of $LiNi_{0.5}Co_{0.2}Mn_{0.3}O_2$ …….. 8

3.2. Electrochemical analysis …….. 8

3.3. Ex-situ structural analysis …… 9

3.3.1. X-ray diffraction …… 9

3.3.2. Transmission electron microscope ……9

3.3.3. Fourier transform infrared spectrometry …… 10
3.3.4. Thermal gravimetric analysis …….. 10
3.3.5. X-ray photoelectron spectroscopy …….. 11
3.3.6. Field-Emission scanning electron microscopy ……11
3.3.7. X-ray absorption spectroscopy ……11

Chapter 4 Results and discussion……..……13
4.1. Effect of charge capacity on electrochemical activity…… 13
4.2. Activation process and de/magnesiation mechanism …….17
4.3. Confirmation of de/magnesiation ……..….30
4.4. Monitoring redox reaction of Ni, Co and Mn ……..... 33

Chapter 5 Conclusion……...……37

Reference

List of Tables

Table 1. The structural data on $LiNi_{0.5}Co_{0.2}Mn_{0.3}O_2$, $Li_{0.25}Ni_{0.5}Co_{0.2}Mn_{0.3}O_2 \cdot 0.24\ H_2O$ and $Mg_{0.05}Li_{0.25}Ni_{0.5}Co_{0.2}Mn_{0.3}O_2 \cdot 0.24\ H_2O$ analyzed using full pattern matching of XRD patterns.

List of Figures

Figure 1. Activation process of $LiNi_{0.5}Co_{0.2}Mn_{0.3}O_2$. Capacity-voltage profiles of NCM – Pt (Ag/AgCl reference electrode) 3 electrode cells charged up to (a) 120 mAh g^{-1} (b) 150 mAh g^{-1} (c) 180 mAh g^{-1} and (d) 220 mAh g^{-1}.

Figure 2. Electrochemical charge/discharge profile of NCM523 electrode in electrolyte consisted of (a) 1M $LiPF_6$ in EC/DMC and (b) 1M $MgSO_4$ in DI water.

Figure 3. X-ray diffraction (XRD) pattern of $LiNi_{0.5}Co_{0.2}Mn_{0.3}O_2$ matched based on the $R\bar{3}m$ by full pattern matching method.

Figure 4. Mechanism of activation process of $LiNi_{0.5}Co_{0.2}Mn_{0.3}O_2$. (a) Ex-situ XRD patterns of NCM523 in a 3-electrode cell during the electrochemical oxidation process. (b) Amplified XRD patterns from E to H in the 2θ range 10-22° and a schematic representation of E and H.

Figure 5. XRD pattern of $Li_{0.25}Ni_{0.5}Co_{0.2}Mn_{0.3}O_2 \cdot 0.24H_2O$ matched based on the R3m.

Figure 6. (a) Ex-situ XRD patterns of $LiNi_{0.5}Co_{0.2}Mn_{0.3}O_2$ in a 3-electrode cell during the discharge and charge process.

Figure 7. Low magnification HR-TEM image of (a) electrochemically synthesized NCM523 and (c) discharged NCM523. High magnification lattice image of surface region where (b) and (d) corresponds to the shaded region in (a) and (c), respectively.

Figure 8. (a) TGA curves and (b) IR spectra of NCM523 during charging and

discharging. The TGA test was conducted at a heating rate of 5 °C min^{-1} under N_2 flow.

Figure 9. TEM-EDS mapping of (a) as-prepared and (b) discharged NCM523. XPS peaks of (c) Mg 2p and (d) C 1s during charging and discharging.

Figure 10. SEM image of (a) as-prepared and (d) full-discharged $LiNi_{0.5}Co_{0.2}Mn_{0.3}O_2$. EDS mapping images of (b), (e) O and (c), (f) Mg, respectively.

Figure 11. XANES spectra of Ni *k*-edge during first (a) charging and (b) discharging, Co *k*-edge during (c) charging and (d) discharging and Mn *k*-edge during (e) charging and (f) discharging.

Figure 12. Schematic figure of activation process and de/magnesiation mechanism of NCM523 in aqueous Mg electrolytes.

Chapter 1. Introduction

1.1 Motivation and outline

To cope with ever-growing demands for wireless electronic devices and environmental issues, it is indispensable to develop efficient energy storage system.[1,2] In this respect, a great deal of attention has been focused on rechargeable battery systems.[3] A LIB system which utilizes Li as a guest ion displays the highest electrochemical performances in terms of power and energy densities among various rechargeable battery systems, enabling its commercialization for small portable devices and mid-sized applications.[4] However, energy density of LIBs is still insufficient for electric vehicles due to the theoretical limitation of the Li guest ion which confines the quantity of charge to one electron per site in electrode materials. To address the energy density issue, exploring new chemistry is required.[5] Multivalent ion battery system is one of the potential candidates, where a guest ion could deliver two or three electrons at one site in the host structure, possibly delivering double or triple capacity than LIBs.[6] Among multivalent ion battery systems, Mg battery has drawn great attention due to non-dendrite characteristic, high volumetric capacity of Mg metal and earth abundant Mg element.[7] However, it suffers from extremely slow kinetics of divalent guest

ions in host materials, which is attributed to strong columbic interaction between divalent guest ions and host ions, delaying the develop of Mg rechargeable battery.[8-13]

Various materials have been investigated to study kinetics of Mg^{2+} ions. Chevrel phases (Mo_6T_8, T = S, Se) are claimed to have an excellent electrochemical activity for Mg^{2+} ions.[14] The high kinetics of Mg^{2+} ions in Chevrel phase is attributed to its unique structure which enable to weaken coulombic interactions between Mg^{2+} and host ions.[15] However, Chevrel phase exhibits low energy density because low polarity of heavy S^{2-} and Se^{2-} anions and Mo^{2+}/Mo^{3+} redox leads to low voltage and low specific capacity.[16-18] Oxide compounds which have large polarity of light O^{2-} anion have also been investigated as an Mg intercalation host to increase voltage and specific capacity. Among oxide compounds, several nano-sized oxides (i.e., spinel-type Mn_2O_4, layered V_2O_5, and layered MoO_3) exhibit an electrochemical activity, delivering higher energy density than Chevrel phase.[19-20] However, the energy density of reported oxides is still insufficient due to relatively low potential of Mn^{3+}/Mn^{4+}, V^{4+}/V^{5+} and Mo^{5+}/Mo^{6+}. High potential and multi redox element is required in Mg cathode materials to increase energy density.

Oxide compounds which utilize Ni as a redox center could be promising

candidates for high energy electrodes because of the high redox potential of Ni and its capability of being a multi redox center.[21-24] Although ternary-layered oxides, $LiNi_xCo_yMn_zO_2$ (NCM), exhibited a high energy density in a LIB system, Mg intercalation in these materials have known to be restricted due to high migration barrier of Mg ions in O3 layered structure. [25,26] Considering that electrode materials containing water molecules (e.g., $MnO_2 \cdot xH_2O$ and $V_2O_5 \cdot xH_2O$) could effectively screen the electrostatic interaction between guest and host ions, intercalation of water molecules into NCM electrode can be an effective way to overcome the sluggish kinetics of Mg^{2+} ions.[27-32] In addition, the synthesis of water-intercalated layered oxides was demonstrated by C. Delmas *et al.* using chemical oxidation method.[33] In this study, we first demonstrate a water-intercalated NCM as a novel high-voltage cathode for Mg batteries. Water-intercalated NCM523 sample was synthesized by electrochemical charging in aqueous Mg electrolytes, and the electrode delivered a high discharge capacity of 190 mAh g^{-1}. It also allows the insertion and extraction of Mg^{2+} ions. In addition, we investigate the phase transformation of NCM523 from O3 to water-intercalated P3 phase and anomalous magnesium insertion reaction mechanism into the P3 phase.

Chapter 2. Research backgrounds

2.1. Introduction to Mg rechargeable batteries

To address environmental issues such as global warming and exhaustion of fossil fuels, eco-friendly renewable energy has been focused. The large-scale energy storage system (ESS) is required to store the energy.[1,2] Among various energy storage technologies, the rechargeable battery system is noted as one of the most significant system due to their high energy density, high energy conversion efficiency and long cycle life characteristic. The most important parameters for ESS is the long cycle life, cost, and high safety of the system. However, LIB system has been limited for use as ESS due to the limited amount of lithium resources and expensive lithium containing precursor as well as safety problems with the lithium dendrite. Therefore, a next-generation secondary battery with low cost, high safety, and high cyclability is required.[3-6]

Mg rechargeable batteries have been long considered as a promising candidate for ESS. High volumetric capacity characteristics with non-dendrite feature of earth-abundant magnesium are advantages to using a magnesium anode. However, it is difficult to use magnesium as the anode due to the

passivation film produced on the surface of the magnesium metal.[16] Hence, the key issue in Mg rechargeable batteries has been the development of anodically stable electrolytes. Secondly, it is a problem that the Mg^{2+} diffusion kinetics in the host material is intrinsically sluggish.[25,26] Prototype systems for Mg rechargeable battery is reported by D. Aurbach et al. in 2000 with a resolution of two issues.[14] Despite of development of non-passivated Mg anode and Mg^{2+} intercalation host, the prototype has several disadvantages with regard to diffusion kinetics and energy density of cathode material. Several researchers have tried to find materials with fast diffusion of Mg^{2+}, high voltage and capacity. However, these cathodes are limited to up to about 500 Wh kg^{-1}.[14-20, 27-32]

2.2 Layered oxides

Positive electrode materials are the main component that determines the performance of the lithium ion battery. The cathode materials in lithium-ion battery system are charged while lithium ions are electrochemically extracted. The laboratory of Professor JB Goodenough was first developed in the O3 type layered oxides of $LiCoO_2$ containing lithium ions.[34] These materials can deliver high theoretical capacity of 270 mAh g^{-1} at over 3.7 V

(*vs.* Li/Li^+).

Layered structure is a structure in which two types of cations are located in the interstitial site between the closed-packed anion planes alternately. The radius and valence state difference between lithium ions as a guest ion and transition metal ions as a redox center in disordered structures can increase the strain energy leading to layered structure. This layered structure can be classified into various layered structures, depending on whether the cations and anions are located in the structure.

In layered oxides, there are various type of layered structure exists such as O3, P3 and O2. To understand the nomenclature, it should be noted Li and transition metal slab. The two oxygen layers and the cations in the interstitial site between two oxygen layers is called slab. The slab can be divided by Li slab and transition metal slab depending on the type of cations in the interstitial site. O and P written before the numbers means that Li interstitial site is octahedral and prismatic site respectively. The numbers written behind O and P means that the number of transition metal or Li slabs in the unit cell. [35]

Materials with various layered structures has been studied as cathode materials. Among them, O3 type layered oxides are widely used due to their high performance. LiCoO2 was used the first time as cathode materials in

O3 type layered oxides. LiCoO2 shows fast rate characteristics and high cyclability. However, LiCoO2 delivers only half of the theoretical capacity due to their oxygen evolution and irreversible phase transformation from O3 to O1 type layered structure where above the half of the Li extracted from the LiCoO2.[36, 37] Many researchers have been tried to replace Co by Ni or Mn ions in LiCoO2 to compensate the disadvantage that represents low practical capacity.[38-41] Three-component layered $LiNi_xCo_yMn_zO_2$ (NCM, $0 < x, y, z < 1$) has exhibited high electrochemical properties. The role of Co, Ni, and Mn ions is to increase power capability, practical capacity and structural stability respectively. Therefore, the battery performance mainly affected by ratio of transition metal ions. Commercially, several NCM layered oxides have been successfully synthesized and adopted to Li-ion battery system.

Chapter 3. Experimental

3.1. Characterization of $LiNi_{0.5}Co_{0.2}Mn_{0.3}O_2$

The $LiNi_{0.5}Co_{0.2}Mn_{0.3}O_2$ sample was supplied by Samsung Fine Chemicals (Daejeon, Korea). The powder sample was analyzed using a X-ray diffractometry (XRD, D2 PHASER, Bruker, Bremen, Germany) equipped with Cu-Kα radiation (λ = 1.54178 Å) at a scanning speed 0.2° min^{-1} in the 2θ range of 10–70°.

3.2. Electrochemical analysis

Tested working electrodes were prepared by the following sequence. A slurry of 70wt% active materials, 20 wt% carbon black (Super-P; Timcal, Bodio, Switzerland), and 10 wt% polyvinylidene fluoride (PvdF) binder, dissolved in N-methyl-1,2-pyrrolidone (NMP, 99.5%; Sigma-Aldrich, St. Louis, Mo, USA), was pasted onto Ti-mesh current collector. NMP was evaporated overnight at 70 °C in a vacuum oven. The individual cells were assembled in the sequence of counter electrode (Pt coil), reference electrode (Ag/AgCl, MF-2052; Bioanalytical Systems, Inc., Germany), working

electrode in a 3 electrode beaker-type cell. The electrolyte consisted of 1M magnesium sulfate ($MgSO_4$) in DI water. The electrochemical performances of all these cells were measured using a potentiogalvanostat (WBCS 3000, WonA Tech, Korea).

3.3. Ex-situ structural analysis

3.3.1. X-ray diffraction

After galvanostatic measurement at different SOCs, 17 electrodes were collected for analysis of structural evolution. The electrodes were disassembled from 3 electrode beaker-type aqueous cells, rinsed with DI water several times, and dried at 70 °C in a vacuum oven for X-ray diffraction (XRD) measurements. Lattice parameters of electrodes were determined by the Full pattern match method using Fullprof software.

3.3.2. High-Resolution transmission electron microscope

The electrodes was scratched and collected. Particles collected were dispersed in ethanol using a sonicator before being transferred onto a lacey C

supported Cu grid. The grids were dried at 70 ℃ in a vacuum oven for high-resolution transmission electron microscope (HR-TEM, JEM-2100F; JEOL, USA). HR-TEM images and energy-dispersive X-ray spectroscopy (EDS) mapping of the samples were measured using a 200-kV TEM. HR-TEM images was recorded to verify structural transformation. EDS mapping was used to confirm intercalation of Mg^{2+}. The electron beam exposure time on the sample was minimized due to thermally instable charged sample.

3.3.3. Fourier transform infrared spectrometry

Fourier transform infrared (FTIR, Hyper ion 3000) spectroscopy analysis was performed on a pellet made of the collected particles from electrodes and KBr powder at Ar atmosphere.

3.3.4. Thermal gravimetric analysis

Samples at as-prepared, 1st charged and discharged were characterized for identifying water molecules in the structure using Thermal gravimetric analysis (TGA, Q-5000 IR, TA Instruments, USA). The TGA analysis of the samples was carried out at a heating rate of 5 °C min^{-1} under N_2 flow.

3.3.5. X-ray photoelectron spectroscopy

X-ray photoelectron spectroscopy (XPS, Sigma Probe) measurements were conducted at as-prepared, 1st charged, discharged and 2nd charged electrodes using Al-K_α radiation. Surface of the sample was sputtered with an argon ion beam for confirmation of insertion of Mg^{2+}. The energy scale of all samples were calibrated using C-C bond of C 1s region at 285 eV.

3.3.6. Field-Emission scanning electron microscopy

Scanning electron microscopy energy-dispersive X-ray spectroscopy (SEM-EDS) mapping analysis were conducted to estimate existence of magnesium in the particles. To clarify insertion of magnesium, focused ion beam technology was used for the particles of the samples.

3.3.7. X-ray absorption spectroscopy

The valence states of Ni, Co and Mn in the structure of the samples were estimated using X-ray absorption near edge structure analyses. The XANES

spectra were obtained from Beamline 8C at the PAL, Republic of Korea. The Ni, Co and Mn *k*-edge spectra were collected in transmission mode. XANES spectra of Ni, Co, and Mn metal were obtained as reference spectra simultaneously.

Chapter 4. Results and discussion

4.1. Effect of charge capacity on electrochemical activity

Electrochemical measurements were performed on the NCM523 electrode to synthesize the water-intercalated NCM523 and to evaluate its electrochemical properties using an aqueous 3 electrode beaker-type cell containing 1M Mg sulfate ($MgSO_4$). According to our galvanostatic measurements, we observed significant increment of discharge capacity after critical point of charge capacity. The electrochemical charge profile until 150 mAh g^{-1} is well agreed with the previous reports (Figure 1a and 1b).[24] When we charged it up to 120 and 150 mAh g^{-1}, almost 12% and 20% (~15, 30 mAh g^{-1}) of the charged capacity was obtained during the first discharge. The slope of charge profile over 150 mAh g^{-1} is smaller than in non-aqueous Li electrolyte shown in Figure 2. It indicates that the electrochemical reaction of NCM523 using aqueous Mg electrolytes differ from Li^+ extraction reaction of it in non-aqueous electrolytes. Interestingly, the specific discharge capacity increased dramatically after the critical point of charge capacity (~150 mAh g^{-1}). When we charged it up to 220 mAh g^{-1}, its capacity reached to 86% of the charge capacity (190 mAh g^{-1}) at 3.1 V *vs.*

Mg/Mg^{2+} during the first discharge, which delivers large energy density of 589 Wh kg^{-1}.

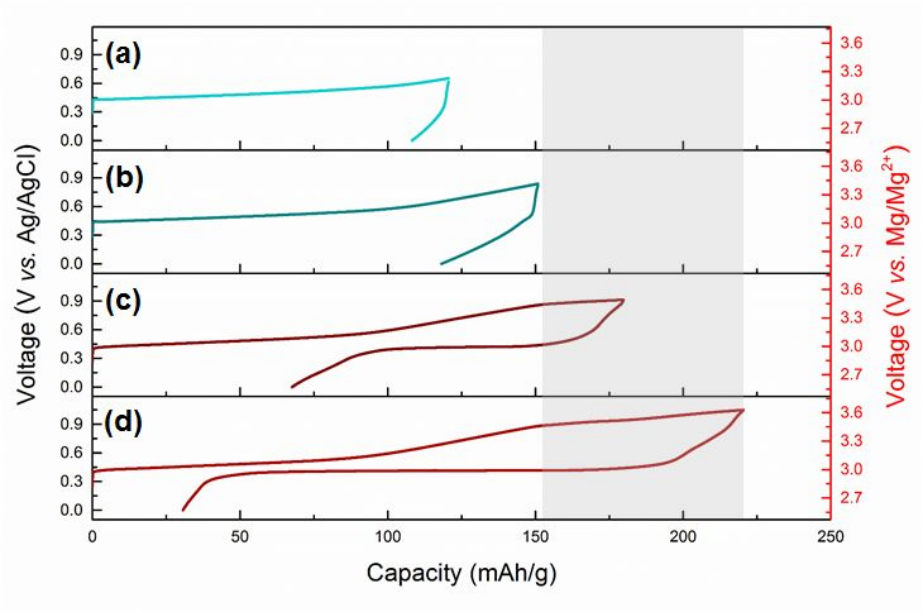

Figure 1. Activation process of $LiNi_{0.5}Co_{0.2}Mn_{0.3}O_2$. Capacity – voltage profiles of NCM523 – Pt (Ag/AgCl reference electrode) 3 electrode cells charged up to (a) 120 mAh g^{-1} (b) 150 mAh g^{-1} (c) 180 mAh g^{-1} and (d) 220 mAh g^{-1}.

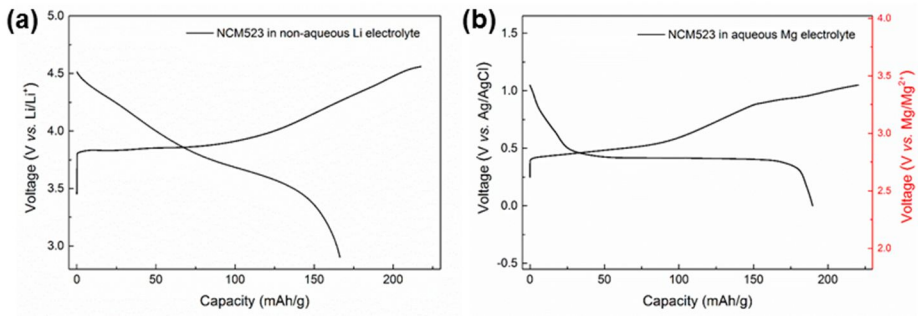

Figure 2. Electrochemical charge/discharge profile of NCM523 electrode in electrolyte consisted of (a) 1M $LiPF_6$ in EC/DMC and (b) 1M $MgSO_4$ in DI water.

4.2. Activation process and de/magnesiation mechanism

Ex situ XRD analysis of the electrodes was conducted at different SOCs to monitor synthesis of water-intercalated NCM523 and structural transformation during magnesiation and demagnesiation in aqueous Mg cell. As-prepared NCM523 is well matched with well-ordered O3 layered structure shown in Figure 3. Figure 4a shows *ex situ* XRD patterns of the electrodes during intermediate charge/discharge states. The characteristic change in the structure can be well identified by observing the (003) Bragg peak positions, as shown in Figure 4b. Slight shifts of the peak were observed from A to E, which is in agreement with previous reports on NCM523 in this region. Following charging to 150 mAh g^{-1}, significantly large full width at half maximum (FWHM: 0.3^{o}) of peaks is observed. Following further extraction of approximately 0.8 Li ion, a new peak arose at a significantly lower angle, about 12.8^{o}, and existing O3 layered peaks disappeared in the XRD patterns. it indicates that a new phase, which has larger c-lattice parameter than O3 phase, is formed.

The unusual large d-spacing value does not correspond to general known transition metal oxides. However, considering cases of hydrated sodium and potassium transition metal oxide and electrochemical reaction of

ion-exchanged intermediate phase ($Na_{0.29}Li_{0.53}Ni_{0.5}Mn_{0.5}O_2$), reaction can involve the intercalation of solvent species into the layered structure.[33, 42] The new phase is corresponds to the structure of P-type cobalt oxyhydroxide in full pattern matching shown in Figure 5. We suggest that the observed new phase is to be P3 phase because O3 phase can transform to P3 phase based on the gliding mechanism of $[Ni_{0.5}Co_{0.2}Mn_{0.3}]O_2$ slabs without breaking TM – O bonds.[43] Broadening of peaks of O3 and P3 phase in the early stage of activation process appears to probably be the result of widening Li slab space and bending and sliding TM slabs, including extraction of Li^+ ions and insertion of H_2O molecules. After the activation process, all ions and H_2O molecules reach their most energetically stable site leading to form well-ordered crystalline P3 structure.

The structural transformation from O3 to P3 phase relates to phase transformation in highly charged state of NCM layered oxides. In Li chemistry, layered oxides with deficient Li contents make unscreend repulsion between opposing oxygen layers in Li slab, resulting in unstable layered phase.[44] To compensate structural instability of Li deficient layered oxides, oxygen evolution and transition metal migration from TM slab to Li slab occurs, which further induces the phase transformation to rock salt and spinel phase at the surface.[45, 46] According to our XRD results, we revealed

that unstable Li deficient NCM523 can be stabilized by water-induced O3 – P3 phase transformation in aqueous Mg system, not oxygen evolution or transition metal migration mechanisms.

The chemical potential and diffusion kinetics of guest ion in P3 phase makes unique charge/discharge profile illustrated in Figure 1, which is different from that of general NCM523. However, the reason of relatively high discharge capacity of water-intercalated NCM523 is not clear whether the changed anion coordination environments of Mg^{2+} ions of transition site originated in structural change or the increased c-lattice parameter by intercalated water molecules.

The magnesiation mechanism of P3 NCM523 can be divided into two steps in the perspective of phase transformation shown in Figure 6. At the first stage of the discharge, slight shifts of the (003), (006) and (015) peaks were observed. It indicates that single phase electrode reaction of P3 NCM523 occurs through the early discharge capacity of 30 mAh g^{-1}. The c-lattice parameter decreased in this solid-solution region, whereas the a- and b-lattice parameter exhibited a negligible change (Table 1). The two-phase reaction appeared during the second stage. Following discharging to 0 V (vs. Ag/AgCl), intensity of all peaks for P3 NCM523 are gradually decreased, while the new peaks are not detected in XRD patterns. The continuously

decreased intensity of the peaks is attributable to structural change from P3 phase to amorphous phase, which is further discussed in the next section. In addition, the discharged phase can be transformed to P3 structure when it is recharged shown in Figure 6.

The structural evolution of NCM523 during electrochemical test was further analyzed using high-resolution TEM (HR-TEM) to directly visualize the local structure of charged and discharged electrodes shown in Figure 7. Figure 7b shows the well-ordered lattice fringe of layered structure in the charged electrode. The d-spacing of the charged P3 phase, gained from the lattice image, was about 6.7 Å, which was similar to those of the (0 0 3) planes of the P3 hydrated layered oxide phase. The TM slabs were waved and wrinkled and the average interslab distances decreased to 3.5-6.8 Å in discharged electrode, which is clearly shown in inset of the figure 7d. This indicates that long-range ordering was completely lost, which corresponds to XRD results. We suggest that decreased c-lattice parameter due to strong attraction between inserted Mg^{2+} and O^{2-} ions squeezed out water molecules into electrolytes, resulting in the decreased interslab distances and waved TM slabs.

We conducted thermal gravimetric analysis (TGA) and Fourier transform infrared spectrometry (FTIR) to further confirm structural

transformation mechanism including insertion and extraction of water molecules during charging and discharging. TGA curve of the charged sample in Figure 8a shows one distinct sloppy region occurring in the range of between 120 and 190°C can be identified to the elimination of water in the crystal.[47, 48] Its total water content is considered to be around 0.24 H_2O molecules per a chemical formula of NCM523. The water content in discharged electrode decreased as expected in TEM results. The water molecules were observed by *ex situ* FTIR spectra during charging and discharging. The IR absorption peaks at 650-400 cm^{-1} range for as-prepared sample typically observed for layered oxides in Figure 8b. Peaks for the two low frequencies are attributable to the O-M-O bending vibration and for the high frequency are attributable to the asymmetric stretching modes of the MO_6 group.[49-51] Peaks at 1500-600 cm^{-1} range are attributable to PvdF binder.[52] With charge reaction, absorption peaks at around 1617 and 3400 cm^{-1} in the FTIR spectra corresponding to the O-H stretching and H-O-H bending modes of crystalline water gradually appeared in the activation region. The results represent that H_2O molecules gradually insert into NCM523 electrode when we charged it from 150 to 210 mAh g^{-1}, which corresponds to HR-TEM image, XRD patterns and TGA data. As it is discharged, intensity of peaks at 1617 and 3400 cm^{-1} decreased. The

concentration of water molecules, which is proportional to the absorbance, decreased which supports the extraction of water molecules out of P3 phase leading to formation of wrinkled layered structure.

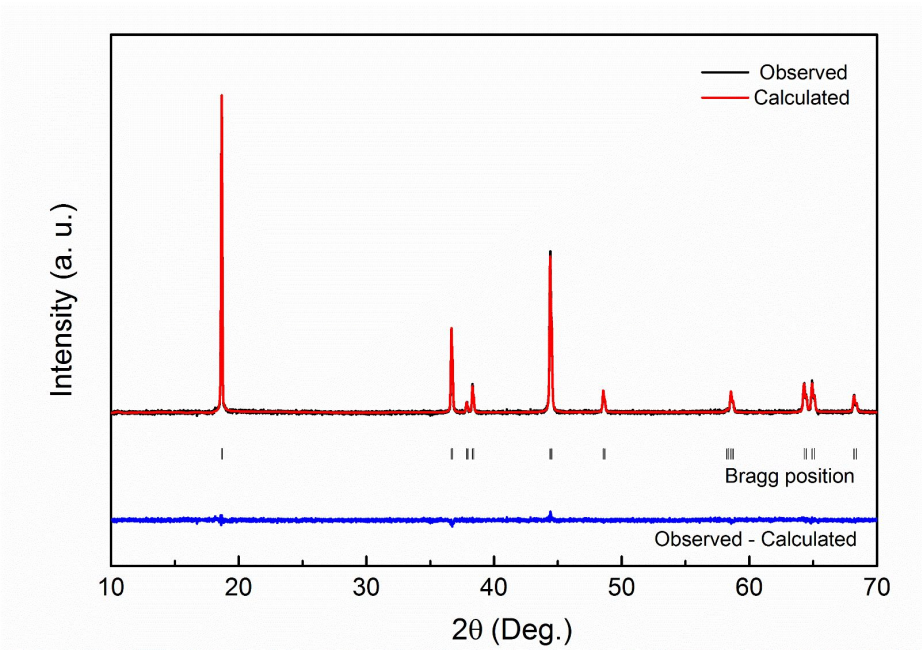

Figure 3. XRD pattern of $LiNi_{0.5}Co_{0.2}Mn_{0.3}O_2$ matched based on the $R\bar{3}m$.

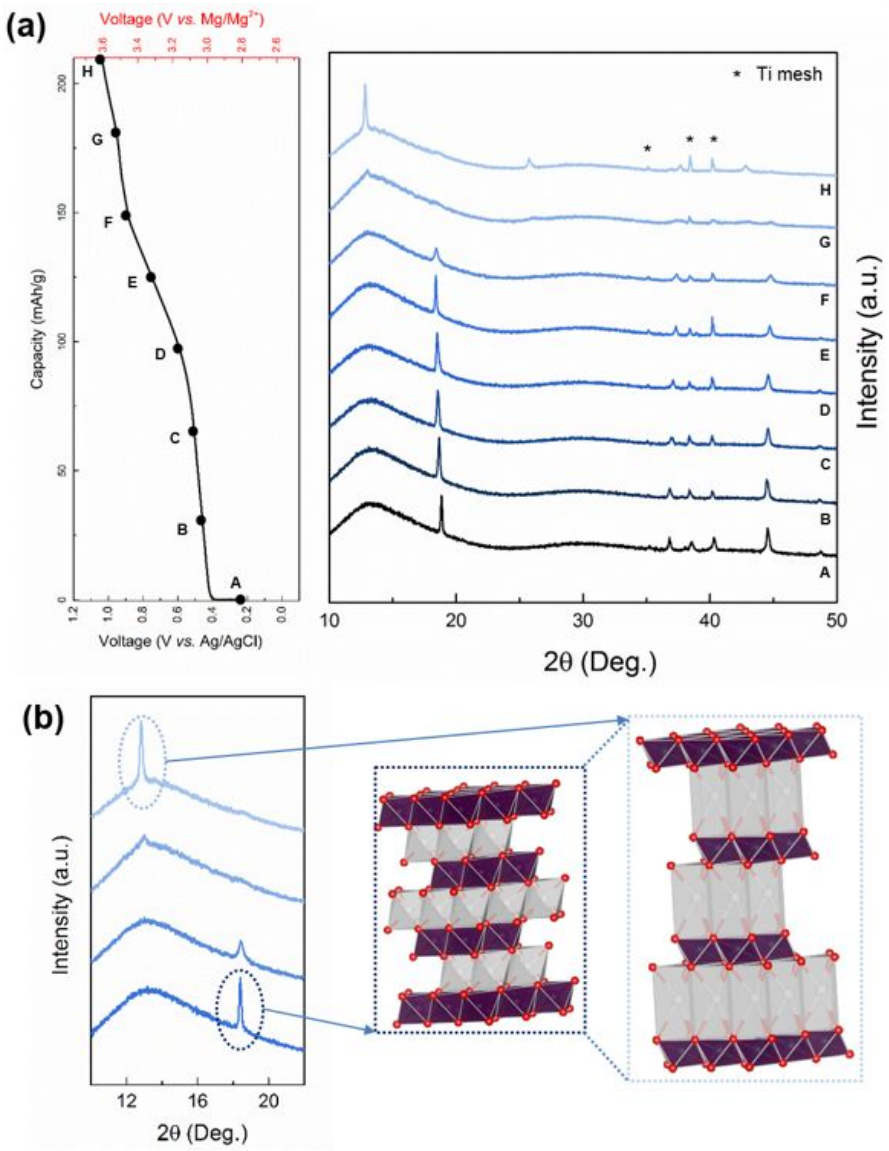

Figure 4. Mechanism of activation process of $LiNi_{0.5}Co_{0.2}Mn_{0.3}O_2$. (a) Ex-situ XRD patterns of NCM523 in a 3-electrode cell during the electrochemical oxidation process. (b) Amplified XRD patterns from E to H in the 2θ range 10-22° and a schematic representation of E and H.

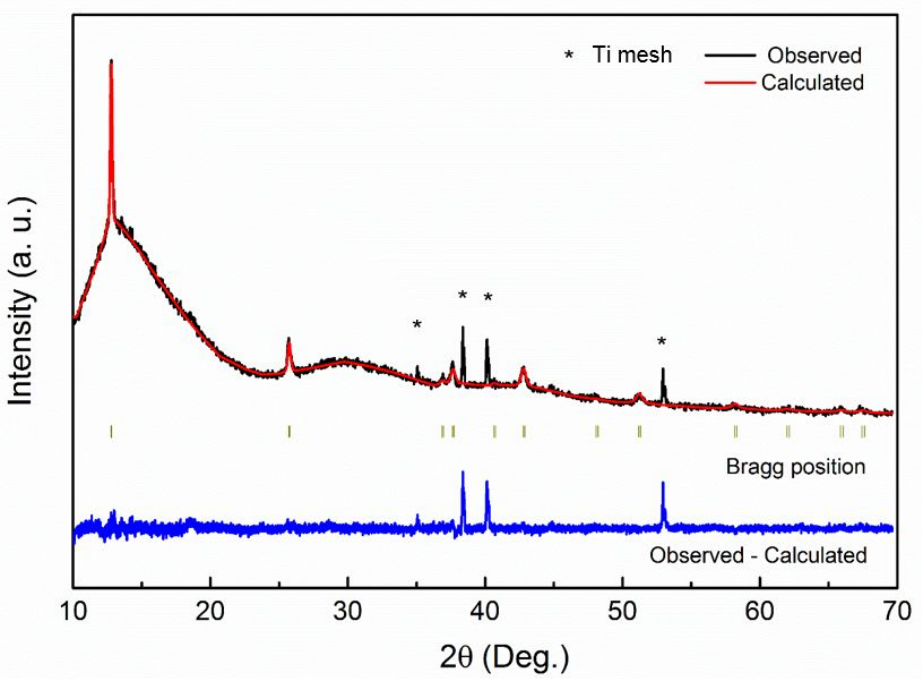

Figure 5. XRD pattern of $Li_{0.25}Ni_{0.5}Co_{0.2}Mn_{0.3}O_2 \cdot 0.24H_2O$ matched on the R3m.

Formula	$LiNi_{0.5}Co_{0.2}Mn_{0.3}O_2$	$Li_{0.25}Ni_{0.5}Co_{0.2}Mn_{0.3}O_2$ ·0.24 H_2O	$Mg_{0.05}Li_{0.25}Ni_{0.5}Co_{0.2}Mn_{0.3}O_2$ ·0.24 H_2O
Crystal system	Rhombohedral	Rhombohedral	Rhombohedral
Space group	$R\bar{3}m$	*R3m*	*R3m*
Lattice parameters			
a (Å)	2.86992 (8)	2.83677 (35)	2.84184 (48)
b (Å)	2.86992 (8)	2.83677 (35)	2.84184 (48)
c (Å)	14.24362 (47)	20.80121 (146)	20.49576 (1070)
Unit cell Volume ($Å^3$)	101.599 (5)	144.966 (27)	143.349 (82)
Source		X-ray	
Temperature (K)		300	
Wave length (Å)		1.54950	
2θ range (°)		10 - 70	

Table 1. The structural data on $LiNi_{0.5}Co_{0.2}Mn_{0.3}O_2$, $Li_{0.25}Ni_{0.5}Co_{0.2}Mn_{0.3}O_2$·0.24 H_2O and $Mg_{0.05}Li_{0.25}Ni_{0.5}Co_{0.2}Mn_{0.3}O_2$·0.24 H_2O analyzed using full pattern matching of XRD patterns.

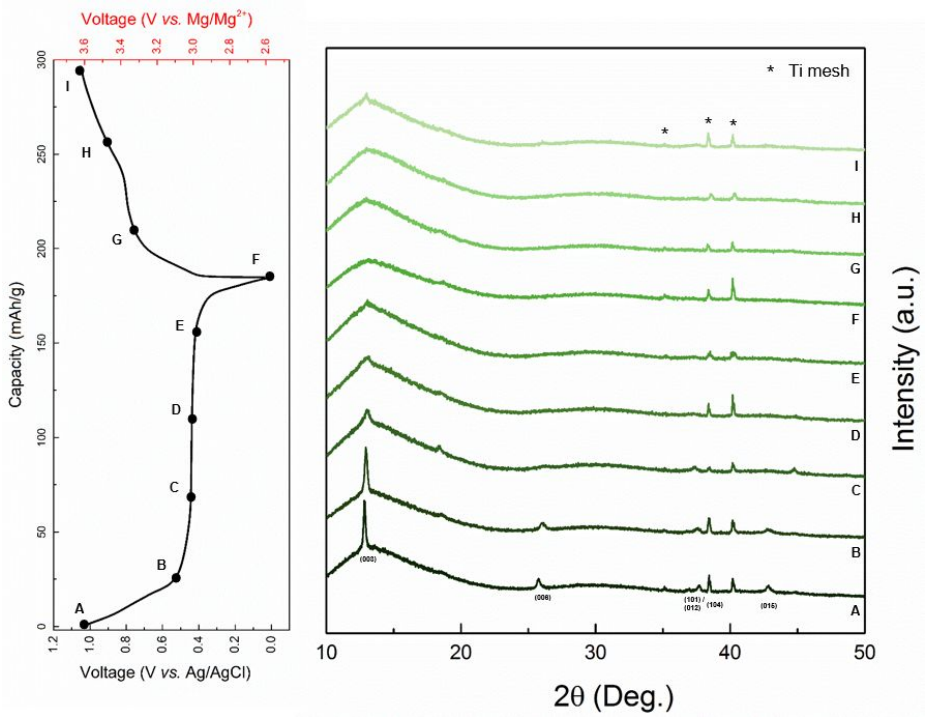

Figure 6. Ex-situ XRD patterns of $LiNi_{0.5}Co_{0.2}Mn_{0.3}O_2$ in a 3-electrode cell during the discharge and charge process.

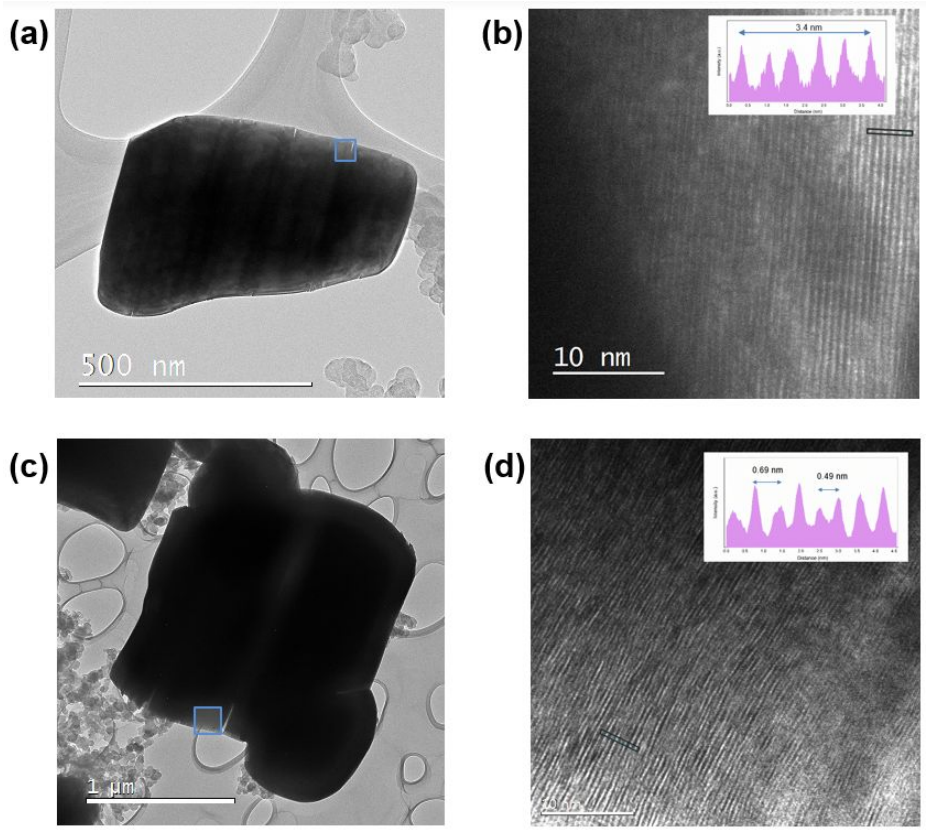

Figure 7. Low magnification HR-TEM image of (a) electrochemically synthesized NCM523 and (c) discharged NCM523. High magnification lattice image of surface region where (b) and (d) corresponds to the shaded region in (a) and (c), respectively.

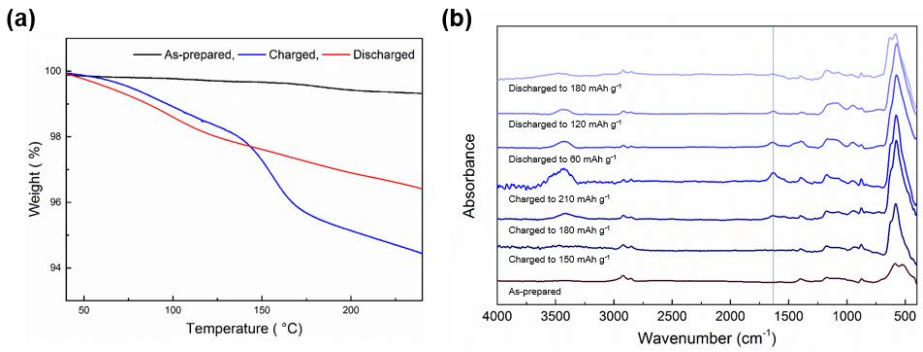

Figure 8. (a) TGA curves and (b) IR spectra of NCM523 during charging and discharging. The TGA test was conducted at a heating rate of 5 °C min^{-1} under N_2 flow.

4.3. Confirmation of de/magnesiation

SEM and TEM energy-dispersive X-ray spectroscopy (EDS) mapping analysis were performed to monitor insertion and extraction of Mg^{2+} ions. Chemical mapping of pristine electrode confirmed that contrary to Ni, Co and Mn ions, Mg ions do not exist in the particle shown in Figure 9a. However, along with the Ni, Co and Mn ions, Mg ions appears in discharged particle in Figure 9b. This result indicates that Mg^{2+} ions insert into P3 phase during discharge process. This is clearly shown in SEM-EDS mapping result at cross-section of NCM523 particles shown in Figure 10. *Ex situ* X-ray photoelectron spectroscopy (XPS) at as-prepared, first charged, first discharged, and recharged states shown in Figure 9c and 9d was further confirmed the reversible Mg^{2+} insertion and extraction in NCM523. In the Mg 2p (at ~50.3 eV) spectra shown in Figure 9c, left and right shift of the Mn 3p (at~49.4 eV) peak is detected due to the evolution of Mg peak with the discharged electrode and vanished Mg peak with recharged electrode.[53, 54] It indicates that insertion and extraction of Mg^{2+} ion occurs during discharge and recharge process. De/magnesiation is clearly observed by Mg KLL (at about 308 eV) auger peak shown in Figure 9d.[55]

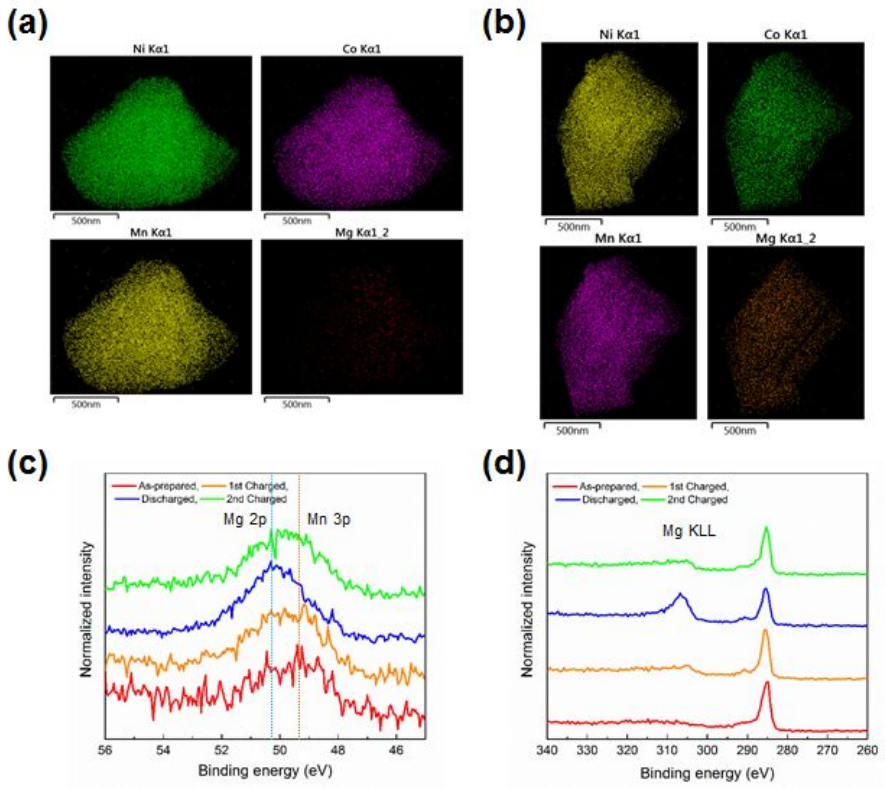

Figure 9. TEM-EDS mapping of (a) as-prepared and (b) discharged NCM523. XPS peaks of (c) Mg 2p and (d) C 1s during charging and discharging.

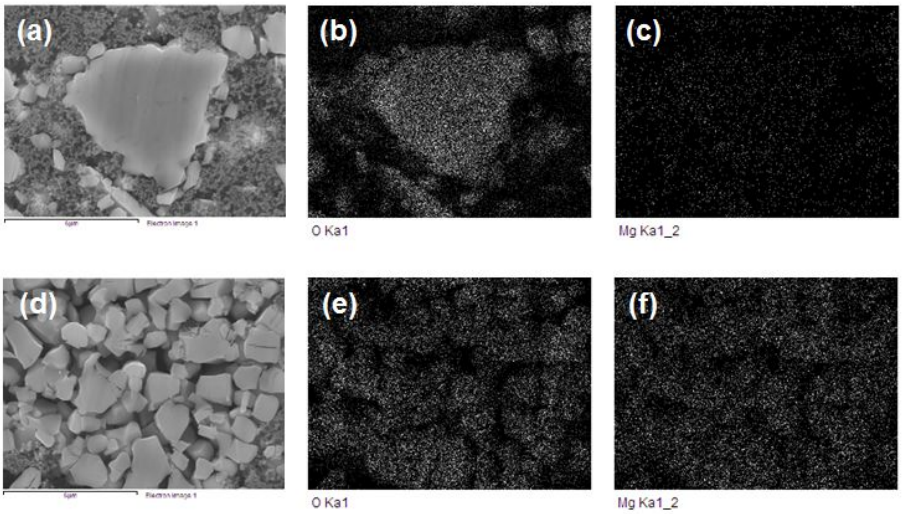

Figure 10. SEM image of (a) as-prepared and (d) full-discharged $LiNi_{0.5}Co_{0.2}Mn_{0.3}O_2$. EDS mapping images of (b), (e) O and (c), (f) Mg, respectively.

4.4. Monitoring redox reaction of Ni, Co and Mn

The redox reaction of NCM523 with Mg^{2+} ions during electrochemical charging and discharging was analyzed using XAS to monitor the oxidation state of Ni, Co and Mn. Figure 11a, 11c and 11e show XANES spectra of the $Li_{1-x}Ni_{0.5}Co_{0.2}Mn_{0.3}O_2 \cdot yH_2O (0 \leq x \leq 0.75, 0 \leq y \leq 0.24)$ electrodes during the first charge process. The Ni K-edge XANES spectrum shows a clear rightward shift up to x = 0.75, which is indicative of change in oxidation state to Ni^{3+} and then to Ni^{4+}. The Co and Mn K-edge XANES spectrum shows little change of the oxidation states of Mn^{4+} and Co^{3+} during charging. The Ni K-edge XANES spectrum shifted leftwards to the initial valence state and gradually changed leading to an isosbestic point at 8354 eV, which appears generally in two-phase electrode materials, during the discharge process in Figure 11b.[56, 57] XANES spectra supports that P3 phase transformed to the waved layered structure which corresponds with XRD and TEM. The Co and Mn K-edge XANES spectrum display that little change in valence states of Co^{3+} and Mn^{4+}. This is first report which used Ni redox center leading to the highest redox potential among Mg cathodes yet reported. Based on the results from above, we present that P3 phase NCM523, which is synthesized in aqueous Mg electrolytes, has electrochemical activity, whereas

O3 phase NCM523 has little electrochemical activity, which were depicted in Figure 12.

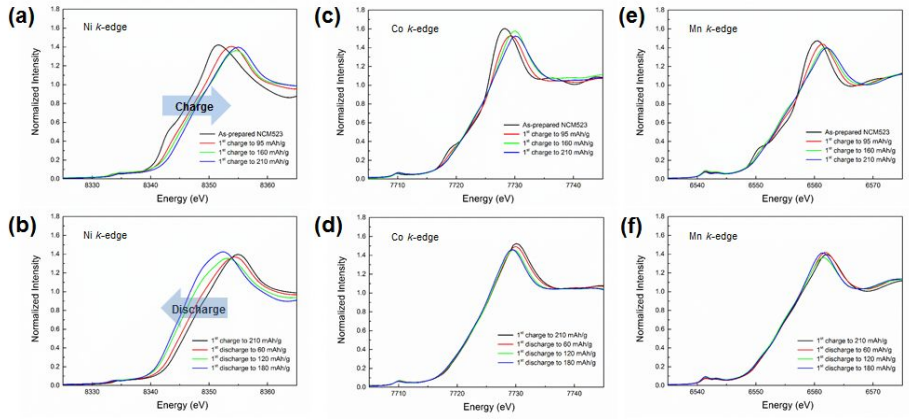

Figure 11. XANES spectra of Ni K-edge during first (a) charging and (b) discharging, Co K-edge during (c) charging and (d) discharging and Mn K-edge during (e) charging and (f) discharging.

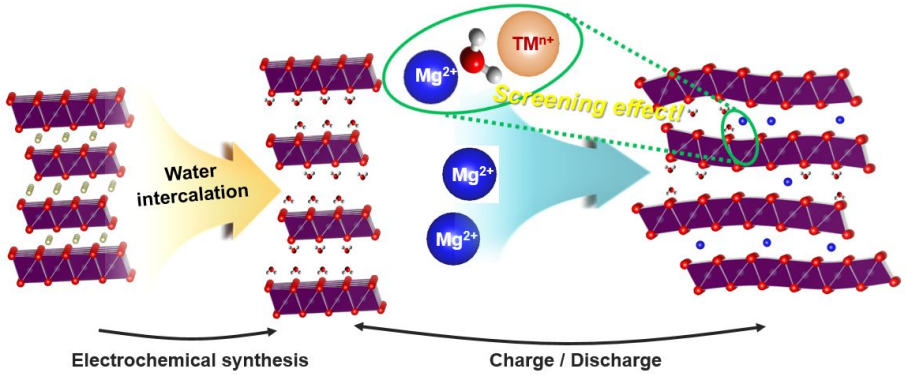

Figure 12. Schematic figure of activation process and de/magnesiation mechanism of NCM523 in aqueous Mg electrolytes.

Chapter 5. Conclusion

In conclusion, a novel P3 phase NCM523 material having water molecules with large c-lattice parameter was successfully prepared by electrochemical delithiation process in aqueous electrolyte containing $MgSO_4$. The P3 phase NCM523 delivers ~190 mAh g^{-1} at 3.1 V *vs.* Mg/Mg^{2+}. The discharge mechanism of the P3 NCM523 is divided into one phase region and two phase region. Insertion of Mg^{2+} ions is accompanied with extraction of water molecules during the two phase reaction from P3 phase to wrinkled layered structure. The strong attraction between inserted Mg^{2+} and O^{2-} ions probably squeezed out water molecules, forming wrinkled layered structure. The $Ni^{2+}/Ni^{3+}/Ni^{4+}$ redox potential of 3.1 V *vs.* Mg/Mg^{2+} is the highest reported among Mg battery cathodes and firstly report using Ni redox during magnesiation. We believe the strategy, which enables layered oxides to insert and extract Mg^{2+} ions through synthesizing water-intercalated layered oxide, makes high energy density Ni based layered oxides promising cathode for Mg rechargeable batteries.

Reference

[1] M. Armand, J.-M. Tarascon, *Nature* **2008**, *451*, 652;

[2] Y.-M. Chiang, *Science* **2010**, *330*, 1485.

[3] T. H. Kim, J. S. Park, S. K. Chang, S. Choi, J. H. Ryu, H. K. Song, *Adv. Energy Mater.* **2012**, *2*, 860.

[4] K. Kang, Y. S. Meng, J. Bréger, C. P. Grey, G. Ceder, *Science* **2006**, *311*, 977.

[5] J.-M. Tarascon, M. Armand, *Nature* **2001**, *414*, 359.

[6] M. M. Huie, D. C. Bock, E. S. Takeuchi, A. C. Marschilok, K. J. Takeuchi, *Coordination Chemistry Reviews* **2015**, *287*, 15.

[7] H. D. Yoo, I. Shterenberg, Y. Gofer, G. Gershinsky, N. Pour, D. Aurbach, *Energy & Environ. Sci.* **2013**, *6*, 2265.

[8] K. Makino, Y. Katayama, T. Miura, T. Kishi, *J. Power sources* **2001**, *99*, 66;

[9] T. Ichitsubo, T. Adachi, S. Yagi, T. Doi, *J. Mater. Chem.* **2011**, *21*, 11764;

[10] B. Liu, T. Luo, G. Mu, X. Wang, D. Chen, G. Shen, *ACS nano* **2013**, *7*, 8051;

[11] Y. Liang, R. Feng, S. Yang, H. Ma, J. Liang, J. Chen, *Adv. Mater.* **2011**, *23*, 640;

[12] Y. Liu, L. Jiao, Q. Wu, Y. Zhao, K. Cao, H. Liu, Y. Wang, H. Yuan, *Nanoscale* **2013**, *5*, 9562;

[13] Y. Liu, L. Jiao, Q. Wu, J. Du, Y. Zhao, Y. Si, Y. Wang, H. Yuan, *J. Mater. Chem. A* **2013**, *1*, 5822.

[14] D. Aurbach, Z. Lu, A. Schechter, Y. Gofer, H. Gizbar, R. Turgeman, Y. Cohen, M. Moshkovich, E. Levi, *Nature* **2000**, *407*, 724.

[15] E. Levi, Y. Gofer, D. Aurbach, *Chem. Mater.* **2009**, *22*, 860.

[16] M. Levi, E. Lancri, E. Levi, H. Gizbar, Y. Gofer, D. Aurbach, *Solid State Ionics* **2005**, *176*, 1695;

[17] G. Suresh, M. Levi, D. Aurbach, *Electrochim. Acta* **2008**, *53*, 3889;

[18] D. Aurbach, G. S. Suresh, E. Levi, A. Mitelman, O. Mizrahi, O. Chusid, M. Brunelli, *Adv. Mater.* **2007**, *19*, 4260.

[19] C. Kim, P. J. Phillips, B. Key, T. Yi, D. Nordlund, Y. S. Yu, R. D. Bayliss, S. D. Han, M. He, Z. Zhang, *Adv. Mater.* **2015**, *27*, 3377;

[20] G. Gershinsky, H. D. Yoo, Y. Gofer, D. Aurbach, *Langmuir* **2013**, *29*, 10964.

[21] T. Ohzuku, A. Ueda, M. Nagayama, *J. Electrochem. Soc.* **1993**, *140*, 1862;

[22] J.-H. Kim, S.-T. Myung, C. Yoon, S. Kang, Y.-K. Sun, *Chem. Mater.* **2004**, *16*, 906;

[23] J. Xiao, X. Chen, P. V. Sushko, M. L. Sushko, L. Kovarik, J. Feng, Z. Deng, J. Zheng, G. L. Graff, Z. Nie, *Adv. Mater.* **2012**, *24*, 2109.

[24] T. Ohzuku, Y. Makimura, *Chem. Lett.* **2001**, 642.

[25] Y.-K. Sun, S.-T. Myung, B.-C. Park, J. Prakash, I. Belharouak, K. Amine, *Nat. Mater.* **2009**, *8*, 320.

[26] Z. Rong, R. Malik, P. Canepa, G. Sai Gautam, M. Liu, A. Jain, K. Persson, G. Ceder, *Chem. Mater.* **2015**, *27*, 6016.

[27] R. Zhang, X. Yu, K.-W. Nam, C. Ling, T. S. Arthur, W. Song, A. M. Knapp, S. N. Ehrlich, X.-Q. Yang, M. Matsui, *Electrochem. Commun.* **2012**, *23*, 110;

[28] S. Rasul, S. Suzuki, S. Yamaguchi, M. Miyayama, *Electrochim. Acta* **2012**, *82*, 243;

[29] D. Imamura, M. Miyayama, *Solid State Ionics* **2003**, *161*, 173;

[30] D. Imamura, M. Miyayama, M. Hibino, T. Kudo, *J. Electrochem. Soc.* **2003**, *150*, A753.

[31] J. Song, M. Noked, E. Gillette, J. Duay, G. Rubloff, S. B. Lee, *Phys. Chem. Chem. Phys.* **2015**, *17*, 5256;

[32] K. W. Nam, S. Kim, S. Lee, M. Salama, I. Shterenberg, Y. Gofer, J.-S. Kim, E. Yang, C. S. Park, J.-S. Kim, *Nano lett.* **2015**, *15*, 4071.

[33] M. Butel, L. Gautier, C. Delmas, *Solid State Ionics* **1999**, *122*, 271.

[34] K. Mizushima, P. Jones, P. Wiseman, J. Goodenough, *Mater. Res. Bull*. 1980, 15, 783

[35] T. Ohzuku, Y. Makimura, *Chem. Lett.* 2001, 642

[36] T. Ohzuku, A. Ueda, *J. Electrochem. Soc.* 1994, 141, 2972;

[37] G. Amatucci, J. Tarascon, L. Klein, *J. Electrochem. Soc.* 1996, 143, 1114.

[38] T. Liu, S.-X. Zhao, K. Wang, C.-W. Nan, *Electrochim. Acta* 2012, 85, 605;

[39] H. Kitao, T. Fujihara, K. Takeda, N. Nakanishi, T. Nohma, *Electrochem. Solid-State Lett.* 2005, 8, A87.

[40] K. W. Nam, S. M. Bak, E. Hu, X. Yu, Y. Zhou, X. Wang, L. Wu, Y. Zhu, K. Y. Chung, X. Q. Yang, *Adv. Funct. Mater.* 2013, 23, 1047.

[41] S. K. Jung, H. Gwon, J. Hong, K. Y. Park, D. H. Seo, H. Kim, J. Hyun, W. Yang, K. Kang, *Adv. Energy Mater.* 2014, 4.

[42] H. Gwon, S.-W. Kim, Y.-U. Park, J. Hong, G. Ceder, S. Jeon, K. Kang, *Inorg. Chem.* **2014**, *53*, 8083.

[43] S. Komaba, N. Yabuuchi, T. Nakayama, A. Ogata, T. Ishikawa, I. Nakai, *Inorg. Chem.* **2012**, *51*, 6211.

[44] J. Choi, A. Manthiram, *J. Electrochem. Soc.* **2005**, *152*, A1714.

[45] K. W. Nam, S. M. Bak, E. Hu, X. Yu, Y. Zhou, X. Wang, L. Wu, Y. Zhu, K. Y. Chung, X. Q. Yang, *Adv. Funct. Mater.* **2013**, *23*, 1047;

[46] S. K. Jung, H. Gwon, J. Hong, K. Y. Park, D. H. Seo, H. Kim, J. Hyun, W. Yang, K. Kang, *Adv. Energy Mater.* **2014**, *4*.

[47] X. Yang, Y. Makita, Z.-h. Liu, K. Sakane, K. Ooi, *Chem. Mater.* **2004**, *16*, 5581;

[48] J. Song, L. Wang, Y. Lu, J. Liu, B. Guo, P. Xiao, J.-J. Lee, X.-Q. Yang, G. Henkelman, J. B. Goodenough, *J. Am. Chem. Soc.* **2015**, *137*, 2658.

[49] S. Ching, D. J. Petrovay, M. L. Jorgensen, S. L. Suib, *Inorg. Chem.* **1997**, *36*, 883;

[50] H. Li, G. Chen, B. Zhang, J. Xu, *Solid state Commun.* **2008**, *146*, 115;

[51] C. Nithya, R. Thirunakaran, A. Sivashanmugam, G. Kiruthika, S. Gopukumar, *J. Phys. Chem. C* **2009**, *113*, 17936.

[52] A. Gupta, R. Bajpai, J. Keller, *J. Polym. Res.* **2008**, *15*, 275.

[53] J. S. Corneille, J.-W. He, D. W. Goodman, *Surf. Sci.* **1994**, *306*, 269;

[54] J. Tsuji, M. Fujita, Y. Haruyama, K. Kanda, S. Matsui, N. Ozawa, T. Yao, K. Taniguchi, *Anal. Sci.* **2005**, *21*, 779.

[55] A. A. Daryakenari, D. Hosseini, T. Saito, A. Apostoluk, C. R. Müller, J.-J. Delaunay, *RSC Adv.* **2015**, *5*, 52578.

[56] Y. Orikasa, T. Maeda, Y. Koyama, H. Murayama, K. Fukuda, H. Tanida, H. Arai, E. Matsubara, Y. Uchimoto, Z. Ogumi, *Chem. Mater.* **2013**, *25*, 1032;

[57] H. Kim, G. Yoon, I. Park, K.-Y. Park, B. Lee, J. Kim, Y.-U. Park, S.-K. Jung, H.-D. Lim, D. Ahn, *Energy & Environ. Sci.* **2015**, *8*, 3325.

국문 요약

마그네슘 이차전지는 이 시스템의 높은 이론 용량과, 낮은 가격 그리고 안정성의 장점으로 인해 차세대 전지로서 많은 관심을 받고 있다. 그러나, 2가 양이온의 마그네슘 이온이 전극 물질의 결정 구조 내에서 이동하는 키네틱이 매우 느리기 때문에 높은 에너지를 가지는 양극 소재를 개발하는 것이 큰 이슈이다. 이 연구에서, 우리는 리튬 이온 배터리에서 가장 성능이 우수하고, 상업적으로 가장 널리 사용하는 물질 중 하나인 $LiNi_{0.5}Co_{0.2}Mn_{0.3}O_2$ (NCM523)물질을 마그네슘 이차전지용 양극소재로서 사용이 가능한지 확인해보았다.

우리는 물이 삽입되어 구조가 O3에서 P3 층상 구조로 변형된 NCM523이 마그네슘의 삽입 및 탈리가 가능한 구조로서 많은 양의 전자 및 마그네슘 이온을 저장할 수 있는 마그네슘 이차전지용 양극소재로서 활용이 가능하다는 것을 확인하였다. 물이 삽입되지 않은 O3 상의 경우 전기화학적 활성도가 거의 없다는 것을 확인하였다. 그러나, 물이 삽입된 P3 상은 $Ni^{2+}/Ni^{3+}/Ni^{4+}$ redox 반응을 하며, 마그네슘 양극 소재로서 589 Wh kg^{-1}의 높은 에너지 밀도를 보였다. P3 상의 NCM523의 방전 메커니즘은 크게 단일상

반응을 하는 구역과 2상 반응을 하는 두 구역으로 나뉘어 진다. 물이 들어가 c축 방향이 크게 늘어난 상에 마그네슘 2가 양이온이 삽입되면서 음이온과의 강한 인력으로 인해 물이 탈리되며 2상 반응을 하는 것을 확인하였다. 물이 탈리되며 원래의 층상구조가 주름지게 되고, 이로 인해 재충전 시 마그네슘 이온의 탈리 반응에 많은 저항이 걸리게 된다. 물을 이용하여 층간 사이를 벌리고 마그네슘 이온의 이동을 쉽게 만들 수 있는 전략을 이용하면, 니켈 기반의 높은 에너지 밀도를 나타내는 층상 구조 산화물이 마그네슘 이차전지용 양극소재로서 적용 가능할 것이라 예상된다.

주요어: 마그네슘 이차 전지, 층상형 산화물, P3상, 물, 마그네시에이션
학 번: 2014-21441